High-spin states and K-forbidden decay in ^{172}Hf

D. M. Cullen,[1,*] C. Baktash,[2] M. J. Fitch,[1] I. Frosch,[2] R. W. Gray,[1] N. R. Johnson,[2] I. Y. Lee,[3] A. O. Macchiavelli,[3] W. Reviol,[4] X.-H. Wang,[1] and C.-H. Yu[1,†]

[1]*Nuclear Structure Research Laboratory, University of Rochester, 271 East River Road, Rochester, New York 14627*

[2]*Physics Division, Oak Ridge National Laboratory, Oak Ridge, Tennessee 37831*

[3]*Lawrence Berkeley Laboratory, Berkeley, California 94720*

[4]*Physics Department, University of Tennessee, Knoxville, Tennessee 37996*

(Received 5 October 1994; revised manuscript received 7 February 1995)

High-spin states were populated in ^{172}Hf with the ^{48}Ca+^{128}Te reaction at 200 and 214 MeV. All of the known rotational bands in ^{172}Hf have been extended and five new rotational bands have been observed using the Gammasphere spectrometer. This study establishes the highest known state in ^{172}Hf at spin $44\hbar$. One of the new bands is a $K^{\pi}=(14^{+})$ strongly coupled rotational band. In conflict with the K-selection rule another newly established bandhead state, with spin $I=K=12$, is observed to γ decay directly to the yrast 12^{+} state. This large breakdown in the K-selection rule ($\Delta K \approx 12$) may be due to a mixing between the low- and high-K states in ^{172}Hf.

PACS number(s): 23.20.Lv, 21.10.Re, 27.70.+q

I. INTRODUCTION

The medium- to heavy-mass hafnium (Hf) isotopes are located in the rare-earth mass region where well-deformed nuclei can be populated to very high spin. Prior to this experiment there were seven known [1–4] rotational bands in ^{172}Hf and the state [4] with the highest excitation energy was at spin $34\hbar$. Consideration of the appropriate Nilsson diagram indicates that there are many available single-particle orbitals around the Fermi surface which could be populated to establish new rotational bands in ^{172}Hf. This and the possibility to extend the known rotational bands to higher excitation energy was the motivation for this study.

The well-deformed Hf nuclei are also special in that they possess a unique set of high-K isomers [5]. Rotational bands built upon these high-K configurations are generally composed of two rotational sequences (signatures) which are connected by intense magnetic dipole ($M1$) transitions and exhibit small signature splitting. These bands are associated with specific single-particle configurations with large Ω and are often referred to as "deformation-aligned" states.

For the mid- to heavy-mass Hf nuclei the presence of near-yrast high-K isomers is not entirely unexpected because there are many high-Ω single-particle orbitals near the Fermi surface. These Hf nuclei are also axially symmetric and the projection of the angular momentum onto the nuclear symmetry axis, K, is an approximately good quantum number at low spin. As a consequence, the K-selection rule governs the decay of these high-K isomeric states such that γ-ray transitions involving large changes in K are hindered. The direct decay from a high-K state to one of the yrast states (which have $K=0$ for even-even nuclei) is not, therefore, expected to occur. However, it is possible that a high-K configuration may have admixtures of low-K components mixed into its wave function or, alternatively, high-K components may become mixed into the wave function of the low-K state it is decaying to. Under these circumstances the decay of a high-K state may become less hindered than predicted by the K-selection rule. This paper reports a direct decay of a $K=12$ strongly coupled bandhead state to the $K=0$ ground-state band. We shall also discuss five other newly established rotational bands in ^{172}Hf and the extensions to the known rotational bands [1–4].

II. EXPERIMENT

High-spin states were populated in ^{172}Hf with the ^{128}Te(^{48}Ca,4n) reaction at 200 and 214 MeV. A thin target of ^{128}Te with mass ≈ 600 μg/cm^2 was used. To prevent the loss of Te atoms when exposed to the beam, and to improve heat conduction and mechanical support, the target had a 400 μg/cm^2 layer of Au deposited on the side facing the beam and 100 μg/cm^2 on the downstream side. The detection system consisted of the Early Implementation of the Gammasphere array at the Lawrence Berkeley Laboratory. The 36 Compton-suppressed germanium detectors were arranged in three rings of five at each of the forward and backward angles of 17.3°, 31.7°, and 37.4° and the remaining six detectors were in a ring at 90° with respect to the beam direction. Double- and higher-fold coincidence events were collected at a rate of 4000 per second with the average fold-per-event being three. A total of 322×10^6 events were collected at 200 MeV and 2540×10^6 unfolded events at 214 MeV.

The data analysis was undertaken with two complementary approaches. A conventional analysis of the double coincidences was first applied. This consisted of unpacking the high-fold coincidence events into their coincident pairs of γ rays and then incrementing these pairs into a two-dimensional matrix. Gates were then placed in this matrix and γ-ray intensities and coincidence relationships were used to determine the order of the γ rays in the level scheme. The Escl8r code [6] was also used to resolve some of the com-

*Present address: Oliver Lodge Laboratory, University of Liverpool, Liverpool L69 3BX, U.K.

†Present address: Physics Division, Oak Ridge National Laboratory, Oak Ridge, TN 37831.

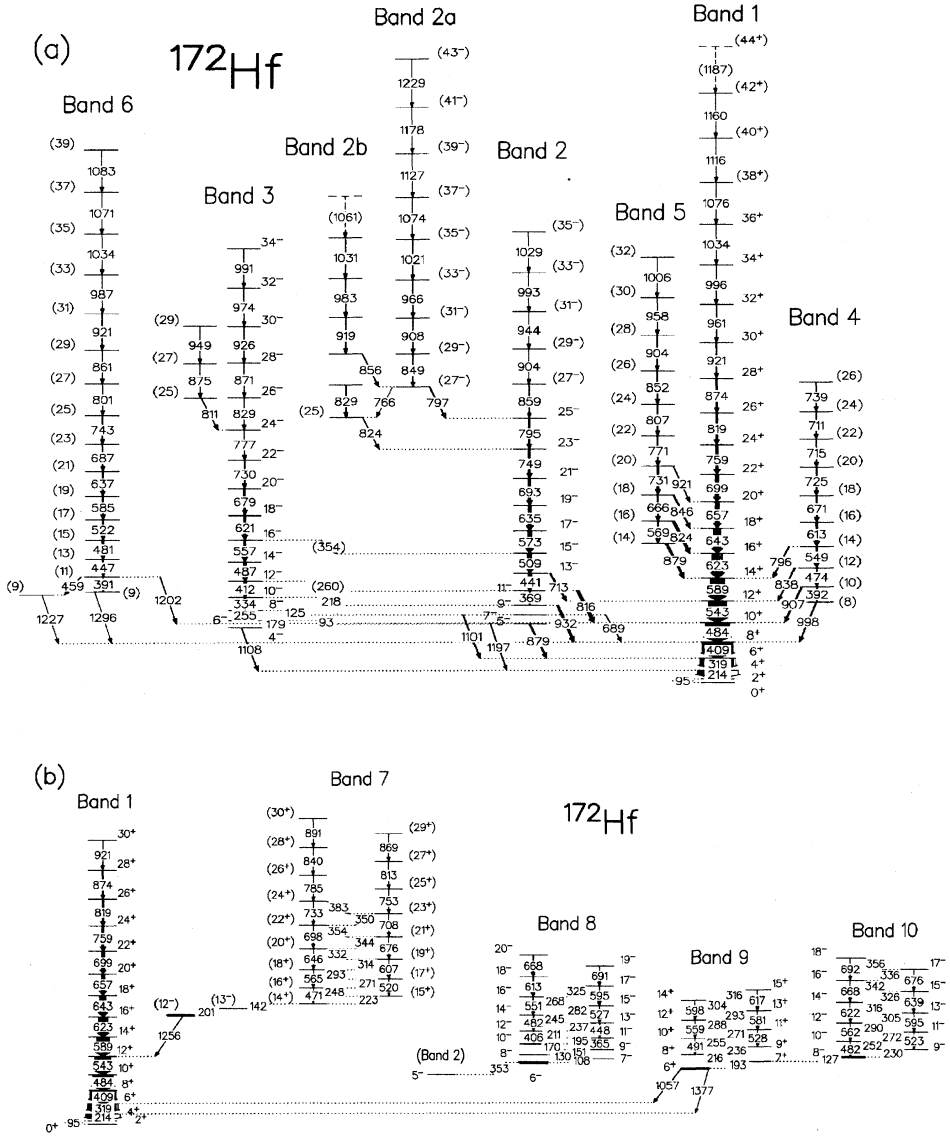

FIG. 1. (a),(b) The level scheme for ^{172}Hf showing the new bands 5 and 6 and a new strongly coupled band 7. The extensions to the known bands 1, 2, 3, 4, band 8 ($K^{\pi}=6^{-}$), band 9 ($k^{\pi}=6^{+}$), and band 10 ($K^{\pi}=8^{-}$) are also shown.

plexities arising from contaminant γ rays and γ rays with the same energy in different bands. In parallel with this approach, these data were also sorted to extract the triple-coincidence events. In this process, gates were placed on the uncontaminated γ rays within a rotational band and a two-dimensional matrix was constructed with the other coincident members of the event. These matrices were invaluable in confirming the level scheme. Finally these data were sorted into a three-dimensional histogram ("a cube") and a full triples analysis was performed to confirm the level scheme using the Levit8r code [6].

The multipolarities of the γ rays were obtained from an angular correlation analysis. A matrix was constructed in which all events in coincidence with one of the six 90° detectors were incremented on one of the axes. The other axis contained those events in coincidence with any other non-90° detector. The directional correlation (DCO) ratios extracted from this matrix were used to confirm the multipolarity of the γ rays except for a few of the weaker transitions.

III. RESULTS

The new level scheme for ^{172}Hf is shown in Fig. 1. In the present study all of the known [1–4] rotational bands in ^{172}Hf (bands 1, 2, 3, 4, 8, 9, and 10) have been extended and five new bands (bands 2a, 2b, 5, 6, and 7) have been established (see Fig. 1). The new band 7 is a high-K strongly coupled rotational band. A new state with $I=K=(12)$ was observed to be in coincidence with band 7. This $K=(12)$ state decays directly to the ground-state band at the $I^{\pi}=12^{+}$ state with a single 1255.9-keV γ-ray transition; see Fig. 1(b). The γ-ray energies and intensities, level energies and spins for all of the transitions in ^{172}Hf are given in Table I. Table II shows the DCO ratios for bands 1, 2, 3, 4 and the newly established bands 5, 6, and 7.

The yrast band 1 has been extended from spin 34^{+} [4] to spin 44^{+} with five new transitions in this work [see Fig. 1(a)]. The DCO ratios for the transitions in band 1 are consistent with those of other known $\Delta I=2$ quadrupole transitions in ^{172}Hf and are shown in Table II. It was not possible

TABLE I. The γ-ray energies and intensities for all the transitions in ^{172}Hf. The uncertainties in the γ-ray energies range from ± 0.15 keV for the strongest to ± 0.5 for the weakest-intensity transitions. The level excitation energies and assigned spins are also shown.

E_γ	I_γ	E_i	E_f	J_i	J_f	E_γ	I_γ	E_i	E_f	J_i	J_f
92.9	0.3(1)	1597.0	1504.1	6^-	5^-	368.9	4.2(2)	2337.6	1968.7	11^-	9^-
95.2	7.8(4)	96.0	0.0	2^+	0^+	383.0	0.31(3)	6774.2	6395.1	(24^+)	(23^+)
108.2	0.4(1)	1966.0	1858.0	7^-	6^-	390.8	0.7(1)	2722.4	2331.7	(11)	(9)
125.1	0.7(1)	1852.3	1727.1	8^-	7^-	391.5	1.7(1)	2428.3	2035.7	$(10,12^+)$	$(8,10^+)$
126.8	0.1(1)	2006.0	1879.0	8^-	7^+	406.5	1.1(1)	2823.4	2417.0	12^-	10^-
129.8	0.7(1)	2096.0	1966.0	8^-	7^-	409.1	90.6(3)	1037.9	628.9	8^+	6^+
142.3	0.5(2)	3662.7	3520.4	(14^+)	(13^-)	411.9	9.2(3)	2598.3	2186.3	12^-	10^-
150.8	0.7(1)	2247.0	2096.0	9^-	8^-	440.7	12.1(5)	2778.6	2337.6	13^-	11^-
170.2	0.7(1)	2417.0	2247.0	10^-	9^-	447.0	3.1(2)	3169.4	2722.4	(13)	(11)
179.1	0.4(1)	1597.0	1417.0	6^-	4^-	448.2	1.5(1)	3060.8	2613.1	13^-	11^-
193.1	0.8(1)	1879.0	1686.0	7^+	6^+	458.8	0.9(1)	2722.4	2263.4	(11)	(9)
195.4	0.5(1)	2613.1	2417.0	11^-	10^-	470.6	0.12(4)	4133.3	3662.3	(16^+)	(14^+)
201.1	0.8(1)	3520.4	3319.3	(13^-)	(12^-)	474.3	1.9(2)	2902.6	2428.3	12^-	10^-
211.1	0.9(1)	2823.4	2613.1	12^-	11^-	481.7	2.1(2)	3305.0	2823.4	14^-	12^-
213.9	100.0(4)	310.0	96.0	4^+	2^+	481.7	6.0(3)	3653.0	3169.4	(15)	(13)
215.9	1.0(1)	2095.0	1879.0	8^+	7^+	482.0	0.4(2)	2488.4	2006.0	10^-	8^-
217.6	0.9(1)	2186.3	1968.7	10^-	9^-	484.1	73.8(2)	1521.8	1037.9	10^+	8^+
222.8	1.3(1)	3885.3	3662.7	(15^+)	(14^+)	487.0	8.6(3)	3085.3	2598.3	14^-	12^-
229.8	0.15(4)	2236.0	2006.0	9^-	8^-	490.9	0.6(1)	2586.0	2095.0	10^+	8^+
236.1	0.8(1)	2331.0	2095.0	9^+	8^+	508.6	13.8(5)	3287.4	2778.6	15^-	13^-
237.1	0.6(1)	3060.8	2823.4	13^-	12^-	519.7	0.1(1)	4405.0	3885.3	(17^+)	(15^+)
244.8	0.4(1)	3305.0	3060.8	14^-	13^-	522.4	3.0(2)	4175.0	3653.0	(17)	(15)
248.1	1.2(1)	4133.3	3885.3	(16^+)	(15^+)	523.0	0.2(1)	2761.0	2236.0	11^-	9^-
252.3	0.33(4)	2488.4	2236.0	10^-	9^-	526.9	1.7(1)	3587.9	3060.8	15^-	13^-
254.6	0.7(1)	2586.0	2331.0	10^+	9^+	528.3	0.22(1)	2857.0	2331.0	11^+	9^+
254.7	3.0(2)	1852.3	1597.0	8^-	6^-	543.5	57.3(2)	2064.3	1521.8	12^+	10^+
268.2	0.5(1)	3856.4	3587.9	16^-	15^-	548.5	4.8(3)	3452.4	2902.6	$(14,16^+)$	$(12,14^+)$
270.8	0.9(1)	2857.0	2586.0	11^+	10^+	550.9	1.9(1)	3856.4	3305.0	16^-	14^-
271.2	1.1(1)	4405.0	4133.3	(17^+)	(16^+)	557.3	6.7(2)	3642.2	3085.3	16^-	14^-
271.9	0.34(4)	2761.0	2488.4	11^-	10^-	558.7	0.7(1)	3145.0	2586.0	12^+	10^+
281.7	0.4(1)	3587.9	3305.0	15^-	14^-	562.5	0.1(1)	3050.5	2488.4	12^-	10^-
287.8	0.5(1)	3145.0	2857.0	12^+	11^+	565.1	0.4(1)	4698.5	4133.3	(18^+)	(16^+)
290.1	0.34(9)	3050.5	2761.0	12^-	11^-	568.9	3.1(2)	4101.5	3532.5	(16^-)	(14^-)
292.9	0.5(1)	3438.0	3145.0	13^+	12^+	573.0	12.3(4)	3860.3	3287.4	17^-	15^-
293.5	0.89(5)	4698.5	4405.0	(18^+)	(17^+)	580.5	0.6(1)	3438.0	2857.0	13^+	11^+
304.3	0.2(1)	3741.0	3438.0	14^+	13^+	584.6	3.6(2)	4759.3	4175.0	(19)	(17)
305.5	0.26(4)	3356.9	3050.5	13^-	12^-	589.6	46.4(2)	2654.5	2064.3	14^+	12^+
313.6	0.73(4)	5011.5	4698.5	(19^+)	(18^+)	594.9	2.7(2)	4181.8	3587.9	17^-	15^-
316.3	0.4(1)	4057.0	3741.0	15^+	14^+	595.3	0.2(1)	3356.9	2761.0	13^-	11^-
316.4	0.23(4)	3673.1	3356.9	14^-	13^-	598.0	0.3(1)	3741.0	3145.0	14^+	12^+
319.0	101.1(3)	628.9	310.0	6^+	4^+	607.2	0.8(1)	5011.5	4405.0	(19^+)	(17^+)
325.4	0.2(1)	4181.8	3856.4	17^-	16^-	612.8	2.4(2)	4469.3	3856.4	18^-	16^-
326.2	0.28(4)	3999.4	3673.1	15^-	14^-	613.2	6.1(3)	4065.3	3452.4	$(16,18^+)$	$(14,16^+)$
331.7	0.53(4)	5344.2	5011.5	(20^+)	(19^+)	616.8	0.5(1)	4057.0	3438.0	15^+	13^+
333.7	7.0(3)	2186.3	1852.3	10^-	8^-	621.3	5.9(2)	4264.9	3642.2	18^-	16^-
335.6	0.2(1)	4675.9	4340.6	17^-	16^-	622.0	0.1(1)	3673.1	3050.5	14^-	12^-
342.2	0.13(3)	4340.6	3999.4	16^-	15^-	623.5	33.2(1)	3278.4	2654.5	16^+	14^+
343.6	0.41(3)	5686.9	5344.2	(21^+)	(20^+)	634.5	10.3(4)	4494.3	3860.3	19^-	17^-
350.4	0.13(3)	6395.1	6041.2	(23^+)	(22^+)	636.7	2.8(2)	5395.5	4759.3	(21)	(19)
353.5	1.8(3)	1858.0	1504.1	6^-	5^-	638.9	0.1(1)	3999.4	3356.9	15^-	13^-
354.1	0.7(1)	6041.2	5686.9	(22^+)	(21^+)	642.6	23.4(8)	3920.8	3278.4	18^+	16^+
355.7	0.15(5)	5032.8	4675.9	18^-	17^-	646.2	0.4(1)	5344.2	4698.5	(20^+)	(18^+)
365.4	0.9(1)	2613.1	2247.0	11^-	9^-	656.7	13.4(5)	4577.3	3920.8	20^+	18^+

TABLE I. (*Continued*).

E_γ	I_γ	E_i	E_f	J_i	J_f	E_γ	I_γ	E_i	E_f	J_i	J_f
665.5	3.9(2)	4766.5	4101.5	(18^-)	(16^-)	871.3	0.9(1)	8145.1	7273.3	28^-	26^-
668.6	0.1(1)	4340.6	3673.1	16^-	14^-	873.7	3.9(2)	7725.9	6852.9	28^+	26^+
667.9	1.2(1)	5137.2	4469.3	20^-	18^-	874.7	1.0(1)	8138.4	7260.0	(27)	(25)
671.1	3.4(2)	4735.0	4065.3	$(18,20^+)$	$(16,18^+)$	878.3	5.9(3)	3532.5	2654.5	(14^-)	14^+
675.8	0.4(1)	5686.9	5011.5	(21^+)	(19^+)	880.0	3.5(6)	1504.1	628.9	5^-	6^+
675.8	0.1(1)	4675.9	3999.4	17^-	15^-	891.1	0.20(4)	9292.3	8401.2	(30^+)	(28^+)
678.7	4.3(2)	4942.3	4264.9	20^-	18^-	903.7	0.7(1)	8492.7	7589.0	(29^-)	(27^-)
687.1	1.7(1)	6082.5	5395.5	23^-	21^-	904.2	1.7(1)	8832.5	7928.5	(28^-)	(26^-)
689.3	2.0(3)	1727.1	1037.9	7^-	8^+	906.6	4.2(4)	2428.3	1521.8	$(10,12^+)$	10^+
690.8	0.5(1)	4803.1	4181.8	19^-	17^-	908.3	1.2(1)	9281.3	8374.3	(31^-)	(29^-)
691.8	0.1(1)	5032.8	4340.6	18^-	16^-	918.6	0.5(1)	9300.4	8381.8	(31^-)	(29^-)
692.8	7.6(3)	5186.6	4494.3	21^-	19^-	920.8	3.2(2)	8645.7	7725.9	30^+	28^+
698.3	0.5(1)	6041.2	5344.2	(22^+)	(20^+)	921.2	1.1(1)	5497.5	4577.3	(20^-)	20^+
699.1	11.5(4)	5276.1	4577.3	22^+	20^+	921.2	0.8(1)	9409.7	8488.7	(31)	(29)
708.3	0.5(1)	6395.1	5686.9	(23^+)	(21^+)	926.0	0.8(1)	9071.8	8145.1	30^-	28^-
710.8	1.5(1)	6885.4	6174.6	$(24,26^+)$	$(22,24^+)$	931.7	6.5(5)	1968.7	1037.9	9^-	8^+
713.7	4.0(2)	2778.6	2064.3	13^-	12^+	943.5	0.6(1)	9436.2	8492.7	(31^-)	(29^-)
715.2	1.4(1)	6174.6	5459.4	$(22,24^+)$	$(20,22^+)$	948.6	0.5(1)	9087.6	8138.4	(29)	(27)
724.6	2.8(2)	5459.4	4735.0	$(20,22^+)$	$(18,20^+)$	958.4	1.2(1)	9790.5	8832.5	(30^-)	(28^-)
729.9	3.2(2)	5671.4	4942.3	22^-	20^-	960.9	2.2(2)	9606.2	8645.7	32^+	30^+
730.9	5.1(2)	5497.5	4766.5	(20^-)	(18^-)	966.1	1.1(1)	10246.7	9281.3	(33^-)	(31^-)
732.7	0.3(1)	6774.2	6041.2	(24^+)	(22^+)	973.6	0.6(1)	10046.8	9071.8	32^-	30^-
738.9	0.9(1)	7624.3	6885.4	$(26,28^+)$	$(24,26^+)$	983.4	0.6(1)	10281.8	9300.4	(33^-)	(31^-)
742.9	2.0(1)	6825.6	6082.5	(25)	(23)	986.7	0.5(1)	10397.0	9409.7	(33)	(31)
748.5	5.5(2)	5934.3	5186.6	23^-	21^-	991.3	0.5(1)	11038.2	10046.8	34^-	32^-
752.5	0.4(1)	7150.1	6395.1	(25^+)	(23^+)	993.4	0.6(1)	10429.6	9436.2	(33^-)	(31^-)
759.2	8.4(3)	6034.6	5276.1	24^+	22^+	996.8	1.8(2)	10601.0	9606.2	34^+	32^+
766.4	0.4(1)	7526.2	6759.3	27^-	(25^-)	997.8	2.9(1)	2035.7	1037.9	$(8,10^-)$	8^+
770.8	3.9(2)	6268.5	5497.5	(22^-)	(20^-)	1006.0	0.7(1)	10797.9	9790.5	(32^-)	(30^-)
777.0	2.8(1)	6449.3	5671.4	24^-	22^-	1021.2	1.2(1)	11268.0	10246.7	(35^-)	(33^-)
785.0	0.3(1)	7561.2	6774.2	(26^+)	(24^+)	1028.7	0.4(1)	11458.2	10429.6	(35^-)	(33^-)
794.7	4.1(2)	6729.7	5934.3	25^-	23^-	1031.4	0.5(1)	11313.2	10281.8	(35^-)	(33^-)
796.0	2.7(2)	3452.4	2654.5	$(14,16^+)$	14^+	1033.7	0.4(1)	11430.5	10397.0	(35)	(33)
796.7	2.5(2)	7525.2	6729.7	(27^-)	25^-	1034.1	1.5(1)	11636.3	10601.0	36^+	34^+
801.3	1.1(1)	7627.0	6825.6	(27)	(25)	1057.0	1.4(7)	1686.0	628.9	6^+	6^+
807.5	2.7(1)	7076.5	6268.5	(24^-)	(22^-)	1061.3	0.4(1)	12374.5	11313.2	(37^-)	(35^-)
811.4	1.3(1)	7260.0	6449.3	(25)	24^-	1071.0	0.3(1)	12500.4	11430.5	(37)	(35)
813.4	0.3(1)	7964.1	7150.1	(27^+)	(25^+)	1074.1	0.5(1)	12344.2	11268.0	(37^-)	(35^-)
816.5	8.5(4)	2337.6	1521.8	11^-	10^+	1076.1	0.8(1)	12711.3	11636.3	38^+	36^+
819.2	5.8(3)	6852.9	6034.6	26^+	24^+	1082.6	0.3(1)	13583.7	12500.4	(39)	(37)
823.6	7.8(3)	4101.5	3278.4	(16^-)	16^+	1099.7	2.6(4)	1727.1	628.9	7^-	6^+
824.1	1.2(1)	6759.3	5934.3	(25)	23^-	1107.6	1.9(8)	1417.0	310.0	4^-	4^+
828.8	1.9(1)	7273.3	6449.3	26^-	24^-	1116.3	0.6(1)	13829.1	12711.3	40^+	38^+
829.0	1.2(1)	7588.3	6759.3	(27^-)	(25^-)	1127.2	0.4(1)	13471.2	12344.2	(39^-)	(37^-)
838.2	2.2(1)	2902.6	2064.3	$(12,14^+)$	12^+	1159.9	0.4(1)	14990.1	13829.1	42^+	40^+
840.2	0.11(4)	8401.2	7561.2	(28^+)	(26^+)	1178.3	0.3(1)	14649.5	13471.2	(41^-)	(39^-)
846.7	3.6(2)	4766.5	3920.8	(18^-)	18^+	1196.4	1.3(3)	1504.1	310.0	5^-	4^+
849.0	1.7(1)	8374.3	7525.2	(29^-)	(27^-)	1201.7	1.3(1)	2722.4	1521.8	(11)	10^+
851.7	2.8(1)	7928.5	7076.5	(26^-)	(24^-)	1226.7	0.7(3)	2263.4	1037.9	(9)	8^+
856.1	1.7(1)	8381.8	7525.2	(29)	27^-	1229.4	0.2(1)	15878.9	14649.5	(43^-)	(41^-)
859.3	1.2(1)	7589.0	6729.7	(27^-)	25^-	1255.9	0.3(1)	3319.3	2064.3	(12^-)	12^+
861.5	1.2(1)	8488.7	7627.0	(29)	(27)	1296.2	0.6(3)	2331.7	1037.9	(9)	8^+
869.1	0.16(4)	8833.8	7964.1	(29^+)	(27^+)	1377.3	0.3(2)	1686.0	310.0	6^+	4^+

TABLE II. DCO ratios for bands 1, 2, 3, 4, 5, band 6, and the strongly coupled band 7. The symbol >1.0 indicates that the transition was more intense in the forward relative to the 90° spectrum. The symbol <1.0 indicates that the transition was more intense in the 90° relative to the forward spectrum. The symbol ≈ 1.0 indicates that the transition has approximately the same intensity in the 90° as in the forward spectrum. The ‡ for the transitions in band 7 indicate that these ratios were extracted from spectra which were gated on dipole transitions. DCO ratios were not calculated for some transitions since they were too weak and/or heavily contaminated by other γ rays with similar energies. (The weakest-intensity transitions were generally only assigned in the level scheme after a series of double-gated spectra were summed.)

E_γ	DCO ratio (band 1)	Assignment
95.2	1.80±0.25	$E2$
213.9	0.88±0.03	$E2$
319.0	1.21±0.04	$E2$
409.1	1.16±0.03	$E2$
484.1	1.25±0.04	$E2$
543.5	1.25±0.08	$E2$
589.6	1.45±0.08	$E2$
623.5	1.27±0.08	$E2$
642.6	1.08±0.08	$E2$
656.7	1.05±0.11	$E2$
699.1	1.07±0.15	$E2$
759.2	0.93±0.14	$E2$
819.2	0.94±0.18	$E2$
873.7	0.96±0.14	$E2$
920.8	0.91±0.28	$E2$
960.9	1.20±0.38	$E2$
996.8	0.93±0.30	$E2$
1034.1	≈1.0	$E2$
1076.1	≈1.0	$E2$

E_γ	DCO ratio (band 2)	Assignment
368.9	1.15±0.30	$E2$
440.7	0.94±0.14	$E2$
508.6	0.83±0.23	$E2$
573.0	0.90±0.15	$E2$
634.5	0.77±0.17	$E2$
692.8	0.92±0.09	$E2$
748.5	0.87±0.09	$E2$
794.7	0.89±0.08	$E2$
849.0	0.80±0.35	$E2$
908.3	0.87±0.25	$E2$
966.1	1.05±0.34	$E2$
1021.2	1.29±0.46	$E2$
766.4	≈1.0	$(E2)$
824.1	≈1.0	$(E2)$
856.1	≈1.0	$(E2)$
816.5	0.64±0.08	Dipole $(E1)$
931.7	0.50±0.08	Dipole $(E1)$

E_γ	DCO ratio (band 3)	Assignment
125.1	0.35±0.14	Dipole $(M1)$
179.1	1.00±0.26	$E2$
254.7	0.93±0.13	$E2$
333.7	0.99±0.18	$E2$
411.9	0.89±0.14	$E2$
487.0	0.78±0.15	$E2$
557.3	1.00±0.30	$E2$
621.3	0.91±0.16	$E2$
678.7	0.97±0.16	$E2$
729.9	1.06±0.15	$E2$
777.0	0.92±0.13	$E2$
828.8	1.03±0.25	$E2$
871.3	≈1.0	$E2$
926.0	≈1.0	$E2$
811.4	<1.0	(dipole)
874.7	≈1.0	$(E2)$
948.6	≈1.0	$(E2)$

E_γ	DCO ratio (band 4)	Assignment
474.3	1.15±0.25	$E2$
548.5	0.94±0.13	$E2$
613.2	1.00±0.15	$E2$
671.1	1.04±0.19	$E2$
724.6	0.89±0.13	$E2$
710.8	1.26±0.11	$E2$
715.2	1.73±0.21	$E2$
738.9	0.85±0.16	$E2$
796.7	1.04±0.44	ΔI=0, 2
838.2	>1.0	ΔI=0, 2
906.6	0.78±0.10	ΔI=0, 2
997.8	1.17±0.10	ΔI=0, 2

E_γ	DCO ratio (band 5)	Assignment
665.5	0.90±0.16	$E2$
730.9	0.90±0.13	$E2$
770.8	0.97±0.14	$E2$
807.5	0.97±0.17	$E2$
823.6	1.16±0.28	ΔI=0, 2
846.7	0.94±0.28	ΔI=0, 2
851.7	0.82±0.21	$E2$
878.3	1.48±0.33	ΔI=0, 2
904.2	≈1.0	$E2$

E_γ	DCO ratio (band 6)	Assignment
390.8	0.79±0.20	$E2$
447.0	1.05±0.19	$E2$
458.8	1.18±0.34	$E2$
481.7	0.86±0.14	$E2$
522.4	1.33±0.26	$E2$
584.6	1.10±0.16	$E2$
636.7	1.24±0.18	$E2$
687.1	1.04±0.21	$E2$
801.3	1.07±0.20	$E2$
861.5	1.03±0.20	$E2$
1201.7	<1.0	Dipole $(E1)$
1226.7	<1.0	Dipole $(E1)$
1296.2	<1.0	Dipole $(E1)$

E_γ	DCO ratio (band 7)	Assignment
142.3	0.70±0.13‡	($E1$ or $M1$)
201.1	0.91±0.16‡	$M1$
222.8	0.92±0.14‡	$M1$
248.1	0.90±0.25‡	$M1$
646.2	1.4±0.3‡	$E2$
708.3	1.3±0.3‡	$E2$
752.5	1.3±0.3‡	$E2$
1255.9	>1.0‡	ΔI=0 (or 2)

to obtain DCO ratios for the highest-spin transitions due to their small intensities. However, these γ-ray transitions are assumed to be $\Delta I=2$ since they appear to be a smooth extension of the lower-spin collective rotational states. These new transitions establish the first proton band crossing in the yrast band at a rotational frequency, $\hbar\omega=0.49$ MeV (see the discussion in Sec. IV).

The known negative-parity band 2 was also extended in this work from spin 33^- [4] to spin 43^- [see Fig. 1(a)]. However, the new band structure differs from that proposed in Ref. [4] above the 25^- state. From the present work, band 2 was observed to be crossed by a new rotational band, band 2a (849.0, 908.3, 966.1, 1021.2, 1074.1, 1127.2, 1178.3, and 1229.4 keV), which extends from spin 27^- to spin 43^- as shown in Fig. 1(a). The DCO ratio for the 796.7-keV transition which links band 2a to band 2 is consistent with a $\Delta I=2$ assignment. However, this transition lies very close to the 794.7-keV, $\Delta I=2$ transition in band 2; thus making the determination of the DCO ratio difficult. Another sequence (859.3, 903.7, 943.5, 993.4 and 1028.7 keV) was observed to be built upon band 2 from spin 25^- to spin (35^-). This new sequence was only weakly populated in these data and no information about the parity or DCO ratio could be extracted. These transitions were, however, assumed to be $\Delta I=2$ since they appear to be a smooth extension of band 2.

The region where these two bands interact is further complicated by the presence of another band, band 2b [see Fig. 1(a)]. A series of four transitions at 918.6, 983.4, 1031.4, and (1061.3) keV were observed to be in coincidence with an 856.1-keV γ-ray and band 2 below the 25^- state. Although a precise DCO ratio for this linking transition could not be extracted, the intensity of the 856.1-keV γ-ray was at least as large in the forward spectra as in the 90° spectra. Therefore, this transition was assumed to be a $\Delta I=2$ quadrupole transition. In addition, a new sequence of two transitions (824.1 and 766.4 keV) was observed in coincidence with the transitions in band 2 below spin 23^-, but was not in coincidence with the 794.7- and 796.7-keV transitions. The DCO ratios for the 824.1- and 766.4-keV transitions suggest that they are either $\Delta I=0$ or $\Delta I=2$ transitions since these transitions are more intense in the forward relative to the 90° spectra. The fact that the 824.1- and 766.4-keV transitions appear to have $\Delta I=2$ nature is consistent with the spin assignment for the lowest state in band 2a (27^-). The spin of this state was determined from the DCO ratio of the 796.7-keV transition. A new 828.8-keV transition was also observed in coincidence with the 824.1-keV γ ray and also the transitions in band 2 below the 23^- state. No spin and parity information could be extracted for this transition because of its small intensity.

Band 3 was also extended by three transitions (926.0, 973.6, and 991.3 keV) from spin 28^- [4] to spin 34^- in this work [see Fig. 1(a)]. A new sequence of three transitions (811.4, 874.7, and 948.6 keV) was observed in coincidence with band 3 below spin 24^- [see Fig. 1(a)]. The 811.4-keV linking transition was observed to have more intensity in the 90° spectrum relative to the forward spectra and is, therefore, assumed to be a dipole transition. The 874.7- and 948.6-keV transitions have more intensity in the forward spectra relative to the 90° spectra and are assumed to be $\Delta I=2$ quadrupole transitions.

Band 4 was previously established [4] up to the 671.1-keV transition. This study has extended band 4 by four transitions (724.6, 715.2, 710.8, and 738.9 keV) and by one more linking transition (796.0 keV) to the yrast band. Band 4 was also extended to lower spin by the addition of a 391.5-keV transition. This new state was observed to decay to the yrast 8^+ state by a new 997.8-keV linking transition. No parity information was obtained in this study. The DCO ratios for this band and its linking transitions are shown in Table II. The 796.0-, 906.6- and 997.8-keV linking transitions have DCO ratios which are consistent with either $\Delta I=0$ or $\Delta I=2$ transitions in ^{172}Hf. The 838.2-keV linking transition was observed to have at least as much intensity in the forward spectra as in the 90° spectra and is also assumed to be a $\Delta I=0$ or $\Delta I=2$ transition. The bandhead spin of band 4 is, therefore, assumed to be (8) or (10). However, since a $\Delta I=2$ assignment will make band 4 yrast, a $\Delta I=0$ assignment is more consistent with its observed intensity relative to band 1.

The new band 5 consists of nine $\Delta I=2$ transitions which cover the spin range (14,16) to (32,34). A spectrum of a sum of double-gated γ rays on this band is shown in Fig. 2(a). Band 5 was observed to decay to the yrast 14^+, 16^+, 18^+, and 20^+ states. No information about the parity of these levels was obtained in this experiment. The DCO ratios for band 5 and for the linking transitions are shown in Table II. The linking transitions have DCO ratios which are similar to other $\Delta I=0$ or $\Delta I=2$ transitions in ^{172}Hf. If it is assumed that these transitions are $\Delta I=0$ ($\Delta I=2$), then the bandhead spin of band 5 is 14 (16).

The new band 6 consists of fifteen $\Delta I=2$ transitions which cover the spin range from (9) to spin (39). The DCO ratios for these transitions are given in Table II. The level with spin (11) was observed to decay directly to the 10^+ member of the yrast band through a new 1201.7-keV γ-ray transition. The DCO ratio for the 1201.7-keV transition is difficult to establish because of its small intensity. However, this transition is suggested to be a $\Delta I=1$ (dipole) since it is observed to have a larger intensity in the 90° direction than in the forward detectors. The other decay branch of this $I=(11)$ state is to a new $I=(9)$ state with a 458.8-keV γ ray. The DCO ratio for the 458.8-keV transition is consistent with the DCO ratios of other $\Delta I=2$ transitions in this band. This $I=(9)$ state was also observed to be connected to the yrast 8^+ state with a 1226.7-keV γ ray transition. The bandhead state in this band, at spin (9), was observed to decay by a 1296.2-keV transition to the yrast 8^+ state. The DCO ratio for these two linking transitions (1226.7 and 1296.2 keV) were difficult to establish due to their small intensities. However, these transitions are suggested to be $\Delta I=1$ (dipoles) since they have a larger intensity in the 90° relative to the forward detectors. Figure 2(b) shows a spectrum which is double gated on the new band 6 in ^{172}Hf. The spectrum illustrates that the transitions in band 6 are in coincidence with the transitions in the yrast band below spin 20. Furthermore, because the yrast transitions are observed up to spin 20, there must be other linking transitions which were not established in these data due to their low intensity and/or their overlap with γ rays with similar energies. The inset to Fig. 2(b) shows the higher energy part of this spectrum ex-

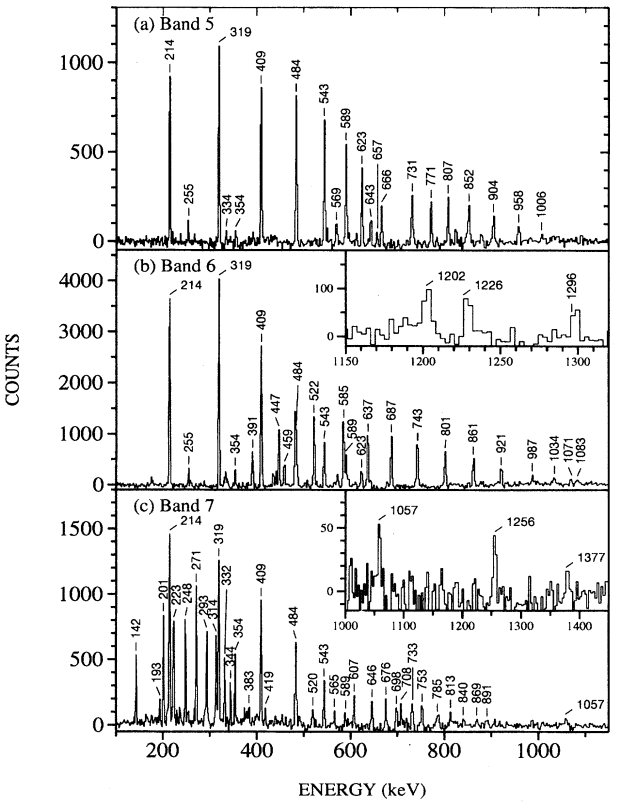

FIG. 2. (a) A sum of 36 double-gated spectra for all the combinations of the transitions 569 to 1006 keV in band 5. Notice the strong coincidence with the yrast transitions (319, 409, 484, 543, 589, 623, 643, and 657 keV). The 255-, 334-, and 354-keV γ-ray transitions are observed to be in coincidence with this band, however, the decay paths to these lower-spin transitions in ^{172}Hf have not been firmly established in the current study. (b) A sum of 105 double-gated spectra for all the combinations of the transitions 391- to 1083-keV in band 6. The inset shows the high-energy part of the spectrum expanded for clarity to show the 1202-, 1227-, and 1296-keV linking transitions. (c) A sum of 66 double-gated spectra for all combinations of the dipole transitions 223- to 383-keV in the strongly coupled band 7. In order to increase the number of counts in this spectrum the 201- and 142-keV transitions, which connect band 7 to the $K^{\pi}=(12^{-})$ bandhead state, were also included in the double-gate list. The yrast band transitions (214, 319, 409, 484, and 543 keV) are observed to be in strong coincidence with these gates. The inset shows the high-energy part of the spectrum expanded for clarity. The 1256-keV γ-ray linking transition is clearly observed. The 193-, 1057-, and 1377-keV transitions from the decay of the known high-K bands are also observed to be in coincidence with band 7 and its decay through the $K^{\pi}=(12^{-})$ bandhead state.

panded to show the three linking transitions (1201.7, 1226.7, and 1296.2 keV).

The new strongly coupled band 7 consists of a sequence of ten dipole $\Delta I=1$ ($M1$) transitions and seven to eight $\Delta I=2$ quadrupole ($E2$) transitions in each signature branch. A spectrum of double-gated γ rays for this band is presented in Fig. 2(c). The DCO ratios for the lower-spin interband transitions could only be obtained from spectra which were gated on dipole transitions (see Table II). These dipole transitions are expected to have some $M1/E2$ mixing components which makes the DCO analysis less effective at distinguishing between dipole and quadrupole transitions. Band 7 is observed to decay to the yrast band through a sequence of three γ-ray transitions, 142.3, 201.1, and 1255.9 keV. The 1255.9-keV transition has a larger intensity in the forward relative to the 90° detectors and the lower limit of the DCO ratio suggests that it is either a $\Delta I=0$ or $\Delta I=2$ transition. In this case the 1255.9-keV transition most likely deexcites from a $K^{\pi}=(12^{-})$ bandhead state (see further discussion of this point in Sec. IV). The DCO ratio for the 201.1-keV transition is consistent with that expected for the first member of the high-K band which is built upon this $K^{\pi}=(12^{-})$ state. The DCO ratio for the 142.3-keV γ ray is consistent with that of a stretched dipole transition with nearly zero mixing ratio. Therefore, it is very likely that this γ ray deexcites the bandhead state of a new $K^{\pi}=(14^{+})$ strongly coupled band 7 to the $I^{\pi}=(13^{-})$ state at 3520 keV excitation energy. These bandhead spin assignments are discussed further in Sec. IV. It should be noted that, similar to the strongly coupled bands in the neighboring nuclei, the $K^{\pi}=(12^{-})$ bandhead state may be isomeric. The presence of an isomeric state could exaggerate the asymmetry in the DCO ratio which could possibly bias the data toward a $\Delta I=0$ or $\Delta I=2$ assignment for the 1255.9-keV transition. This is because the collimators on the non-90° detectors allow these detectors to view a greater length of the recoil path than those on the 90° detectors. As a consequence the forward and backward detectors observe decays which occur outside the focus of the 90° detectors as the recoiling compound nucleus decays downstream from the target.

Nearly 24±9% of the intensity of the $K^{\pi}=(12^{-})$ bandhead state (i.e., the ratio of the total intensities of the 1255.9- and 201.1-keV transitions) decays directly to the yrast 12^{+} state via the 1255.9-keV transition [see Fig. 1(b) and inset to Fig. 2(c)]. This point and its consequences are discussed further in Sec. IV. Some of the remaining intensity of the $K^{\pi}=(12^{-})$ bandhead state most likely decays to the previously established $K^{\pi}=6^{-}$ (band 8), $K^{\pi}=6^{+}$ (band 9), and the $K^{\pi}=8^{-}$ (band 10) strongly coupled bands [1]. For example, when gates are set on the γ-ray transitions in band 7 and on the 201.1 and 142.3-keV γ rays, the transitions that decay from the bandhead of bands 8, 9, and 10 (the 193.1, 1057.0, and 1377.3 keV γ rays) are observed in coincidence [see the inset in Fig. 2(c)]. However, the discrete γ-ray linking transitions to these lower-K bands are not observed since they are individually weaker than the 193.1-, 1057.0-, and 1377.3-keV γ rays where the total γ-ray intensity of the decay is constrained to pass. $B(M1)/B(E2)$ ratios were extracted for a few of the states in band 7 where accurate γ-ray intensity measurements were possible. These ratios are shown in Table III.

Some of the other known [1,3] strongly coupled bands in ^{172}Hf have also been extended. The γ rays in these high-K strongly coupled bands in ^{172}Hf have very similar energies to those of the neighboring nuclei ^{174}Hf [7,8] and ^{176}Hf [9]. Band 8 built upon the $K^{\pi}=6^{-}$ isomer has been confirmed and extended by three ($E2$) transitions on each signature branch to a maximum spin of 20, and by three ($M1$) dipole transitions. Band 9 built upon the $K^{\pi}=6^{+}$ isomer has also been confirmed and extended by two ($E2$) transitions on

TABLE III. Experimental $B(M1)/B(E2)$ ratios for a few of the states in the new strongly coupled band 7 in ^{172}Hf. I_i refers to the spin of the initial state and I_f to the spin of the final state.

I_i ($\hbar$)	I_f ($\hbar$)	E_γ (keV)	$B(M1)/B(E2)$ $(\mu_N/e\text{b})^2$
(18)	(16)	565.1	
	(17)	293.5	3.5±0.5
(19)	(17)	607.2	
	(18)	313.6	1.8±0.2
(20)	(18)	646.2	
	(19)	331.7	2.6±0.4
(21)	(19)	675.8	
	(20)	343.6	2.4±0.4
(22)	(20)	698.3	
	(21)	354.1	3.8±0.7
(24)	(22)	732.7	
	(23)	383.0	2.4±0.5

each signature partner to a maximum spin of 15 and by four dipole connecting transitions. Band 10 built upon the $K^\pi = 8^-$ isomer has been extended by two quadrupole ($E2$) transitions and three dipole ($M1$) transitions. These extensions to the known rotational bands are also shown in Fig. 1.

IV. DISCUSSION

A systematic survey of the neighboring nuclei has been performed in order to establish configurations for the newly established rotational bands in ^{172}Hf. Cranked-shell model (CSM) and total-Routhian-surface (TRS) calculations based on those described in Ref. [10] were performed for ^{172}Hf. The results of the TRS calculation for the vacuum configuration in ^{172}Hf predict that ^{172}Hf has a very stable axially-symmetric deformation which is characterized by ($\beta_2=0.288$, $\beta_4=0.005$, and $\gamma=0.3°$) from low ($\hbar\omega=0$ MeV) to high ($\hbar\omega=0.5$ MeV) rotational frequencies (see Fig. 3). The theoretical quasineutron and quasiproton Routhians for ^{172}Hf, extracted from the CSM calculations performed at this deformation, are shown in Figs. 4(a) and 4(b), respectively. These calculations predict that there are three low-lying neutron orbitals ([633]7/2, [521]1/2, and [512]5/2) just above the $N=100$ Fermi surface. Similarly, the lowest-lying proton orbitals above the $Z=72$ Fermi level are the [514]9/2, [541]1/2, [402]5/2, and [404]7/2 orbitals. Rotational bands built upon these individual and combinations of these orbitals have been established in the neighboring nuclei. In the ensuing discussion the neutron orbitals will be referred to with the standard notation, as given in Table IV.

The experimental alignments, kinematic moments of inertia $\mathcal{J}^{(2)}$, and Routhians for bands 1 through 6 are shown in panels (a), (b), and (c) of Figs. 5 and 6, respectively. From Figs. 5(a) and 5(b) it is evident that the yrast band 1 undergoes the neutron AB band crossing, from the vacuum to both signatures of the $i_{13/2}$, [633]7/2 configuration, at $\hbar\omega=0.32$ MeV with an alignment gain of approximately $6.1\hbar$. This band was also extended to sufficiently high rotational frequency in this work to allow the observation of the first proton band crossing to be established at $\hbar\omega=0.49$ MeV [see Figs. 5(a) and 5(b)]. In the neighboring nucleus ^{174}Hf the neutron AB band crossing in the yrast band takes place at $\hbar\omega=0.31$ MeV with an alignment gain of $6.6\hbar$ and the first proton band crossing is observed to occur at $\hbar\omega=0.51$ MeV [7,8]. In comparison the CSM theoretical quasineutron Routhians in Fig. 4(a) reveal that the AB band crossing is expected to occur at $\hbar\omega=0.24$ MeV in ^{172}Hf. The quasiproton Routhians, Fig. 4(b), predict that the first proton crossing should occur at $\hbar\omega=0.45$ MeV.

The negative-parity bands 2 and 3 have previously been assigned as signature-partner bands which are built upon octupole-vibrational states at low spin [1]. (The spins and parities for the lower-spin states in these bands are adopted from Ref. [1].) The alignment of these bands at low spin is about $3\hbar$ [see Fig. 6(a)] which exceeds that of the yrast band below the AB band crossing [Fig. 5(a)]. With increasing rotational frequency these bands gradually change from an octupole-vibrational structure to a two quasiparticle configuration. Band 2 does not show any evidence for an AB band crossing near $\hbar\omega=0.32$ MeV. This observation, as well as the negative parity of the band and its low-lying Routhian [see Fig. 6(c)] are all consistent with the characteristics of a neutron AE configuration ([633]7/2⊗[521]1/2). However, continuation of band 2 to higher frequencies does not show a clear indication of the expected BC crossing [see Figs. 6(a) and 6(b)]. At a rotational frequency of ≈0.4 MeV, band 2 is crossed by two bands 2a and 2b [see Figs. 6(a) and 6(b)]. Interestingly, band 2a is the only band in this nucleus that does not show the first proton crossing observed in bands 1, 3, and 6 at $\hbar\omega\approx0.5$ MeV. This may suggest a two-quasiproton configuration for this band. (A very similar

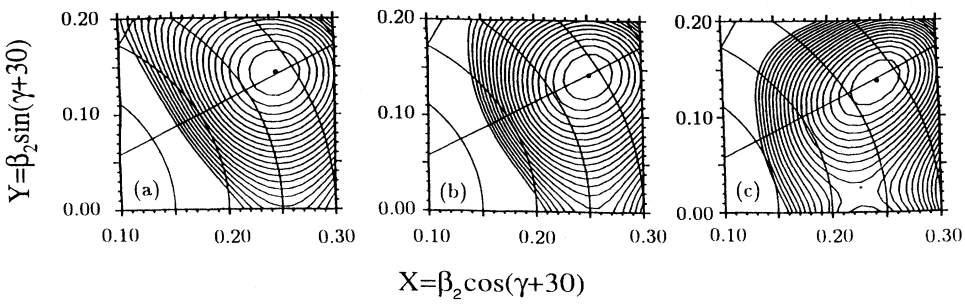

FIG. 3. Results of TRS calculations for ^{172}Hf. These calculations predict that ^{172}Hf has a stable axially-symmetric deformation of ($\beta_2=0.288$, $\beta_4=-0.005$, $\gamma=0.3°$) over a large range of rotational frequency. The figure shows three rotational frequencies corresponding to (a) the low- ($\hbar\omega=0$ MeV), (b) medium- ($\hbar\omega=0.25$ MeV), and (c) high-spin ($\hbar\omega=0.5$ MeV) regions.

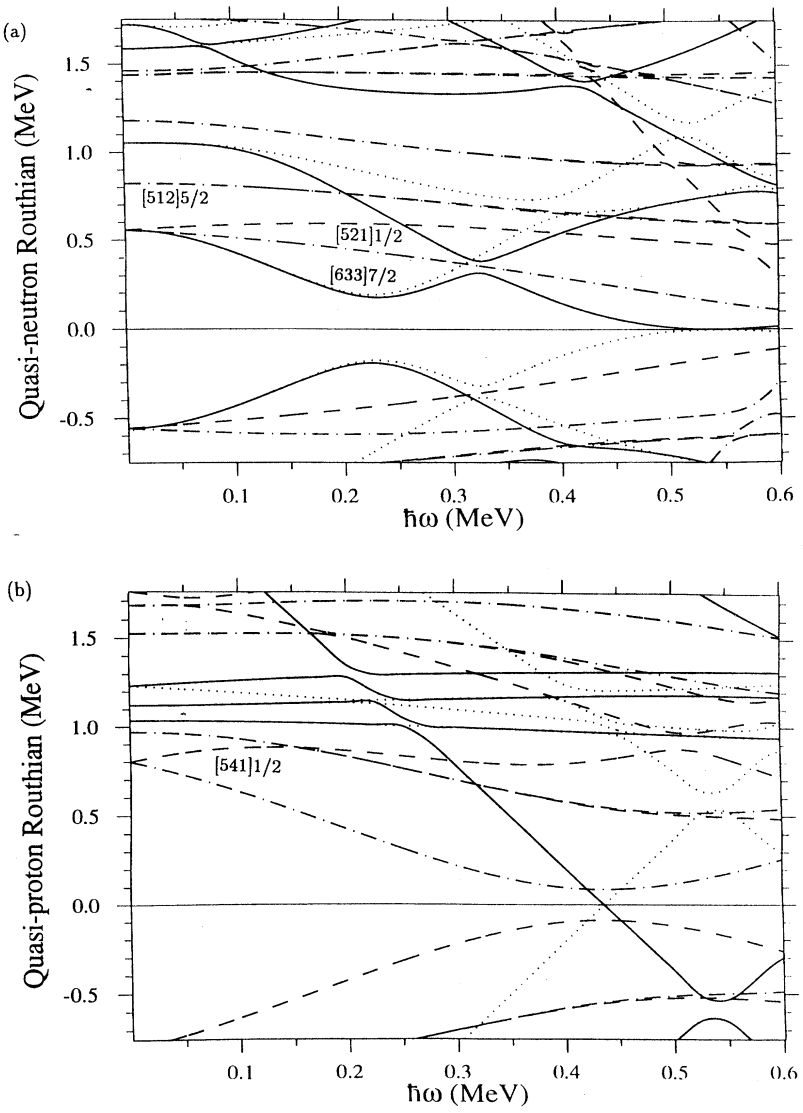

FIG. 4. Routhians from CSM calculations performed at the deformation predicted from the TRS calculation (β_2=0.29, β_4=−0.005, γ=0.3°) for (a) quasineutrons; (b) quasiprotons. The convention for the lines in the plots are: solid lines refer to $(\pi,\alpha)=(+,1/2)$, dotted lines refer to $(\pi,\alpha)=(+,-1/2)$, dash-dotted lines refer to $(\pi,\alpha)=(-,1/2)$, and dashed lines refer to $(\pi,\alpha)=(-,-1/2)$ quantum numbers.

crossing with a weak interaction strength has also been observed in the band based on the [633]7/2 orbital in ^{171}Hf [11].) It may be noted that the γ-ray energies in band 2b are within a few keV of those in band 6. However, lack of reliable DCO information for the 856.1-keV transition prevents definitive spin assignments to be made for this band.

TABLE IV. The labels for the lowest neutron orbitals around the neutron N=100 Fermi surface; n refers to the nth orbit of a particular parity and signature.

Label	Neutron orbit	$(\pi,\alpha)_n$
A	[633]7/2	$(+,+1/2)_1$
B	[633]7/2	$(+,-1/2)_1$
C	[642]5/2	$(+,+1/2)_2$
D	[642]5/2	$(+,-1/2)_2$
E	[521]1/2	$(-,+1/2)_1$
F	[521]1/2	$(-,-1/2)_1$
G	[512]5/2	$(-,+1/2)_2$
H	[512]5/2	$(-,-1/2)_2$

The Routhian for the even-spin, negative-parity band 3 suggests that it is the signature partner to band 2 with a *small signature splitting* [see Fig. 6(c)]. Of the two candidate configurations for this band, namely AF and BE, the latter [633]7/2⊗[521]1/2 configuration seems to be more probable. [The signature splitting between the E and F orbitals shown in Fig. 4(a) is much larger.] Two γ rays 874.7 and 948.6 keV were observed to feed into band 3 at spin 24 (see Fig. 1). However, no spectroscopic information could be obtained regarding the characteristics of this new sequence.

Judging from the quasineutron Routhians shown in Fig. 4(a), we expected to observe another pair of signature-partner bands associated with the AF and BF configurations which would not experience the AB crossing. Since neither of the even-spin bands 4 and 5 show the AB crossing expected at a rotational frequency of about 0.32 MeV, they are both viable candidates for the AF configuration. From Fig. 5(a), it may be seen that band 4 undergoes a sharp crossing at a rotational frequency of 0.36 MeV with an alignment gain

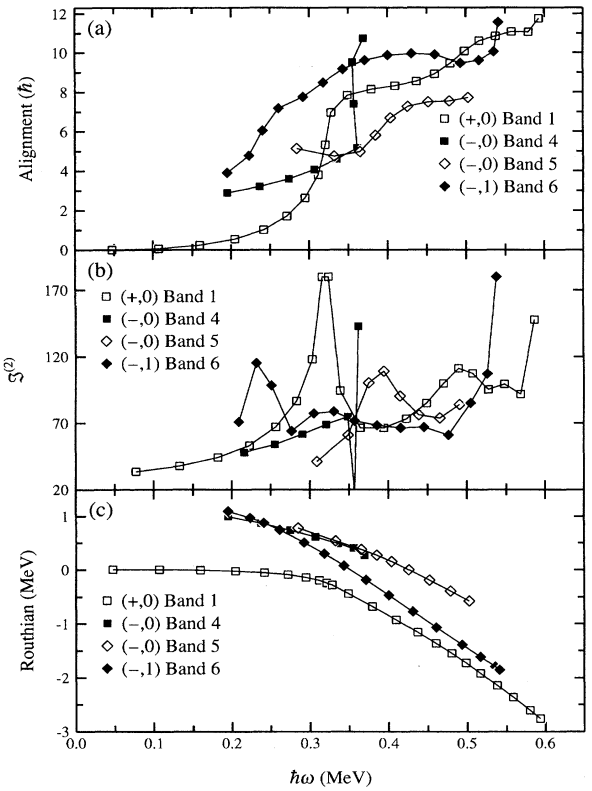

FIG. 5. Plots of experimental (a) alignment; (b) dynamical moments of inertia $\mathcal{J}^{(2)}$; and (c) Routhians for bands 1, 4, 5, and 6 in ^{172}Hf. The Harris parameters $I_0=31.4\hbar^2$/MeV and $I_1=62.7\hbar^4$/MeV^3 were subtracted as a reference band.

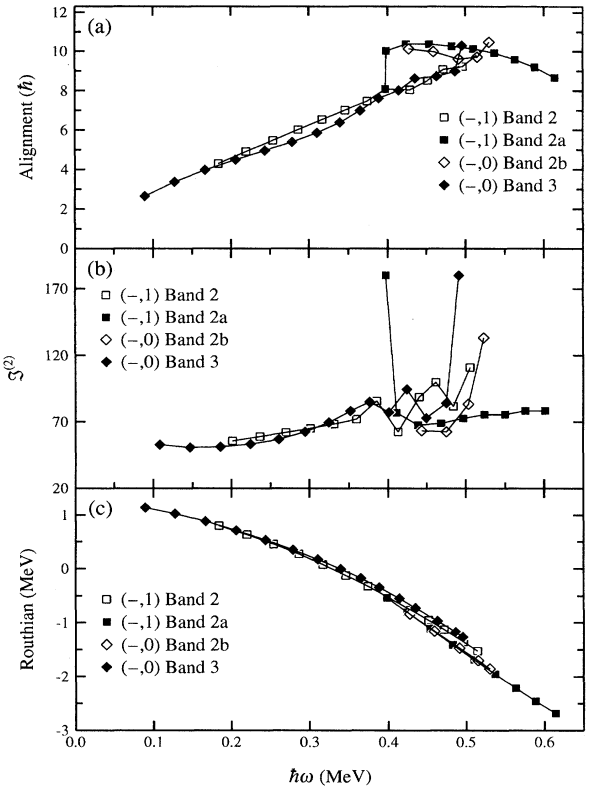

FIG. 6. Plots of experimental (a) alignment; (b) dynamical moments of inertia $\mathcal{J}^{(2)}$; and (c) Routhians for bands 2, 2a, 2b, and 3 in ^{172}Hf. The Harris parameters $I_0=31.4\hbar^2$/MeV and $I_1=62.7\hbar^4$/MeV^3 were subtracted as a reference band.

of about $6\hbar$. The weak interaction strength, as well as the observed crossing frequency and alignment gain of this band are very similar to those for the neutron BC crossing shown in Fig. 4(a). (The BC band crossing is observed to have an alignment gain of $5\hbar$ in the neighboring nucleus ^{170}Hf [12].) In contrast, band 5 shows a band crossing at a frequency of $\approx$0.4 MeV which has a stronger band interaction [see Fig. 5(b)], and results in an alignment gain of about $3\hbar$ [see Fig. 5(a)]. Therefore, we have tentatively assigned band 4 as the AF ([633]7/2⊗[521]1/2) configuration. Further argument in favor of this assignment is that the observed relative alignments and the differences between the Routhians of the bands 2 and 4 are consistent with the expected values for the AE and AF configurations (namely, the large signature splitting associated with the [521]1/2 orbital).

Although the interaction strength and crossing frequency of band 5 are consistent with those of the AD crossing, the tentative signature of this band cannot be reconciled with that of the BF configuration. Consequently, it remains a puzzle as to why the BF configuration has not been observed in this experiment.

The new band 6 does not show any evidence for an AB band crossing at $\hbar\omega=0.32$ MeV although it does exhibit a small bump in its dynamical moment of inertia [Fig. 5(b)] at this rotational frequency. This band does not show any evidence for the next neutron crossing BC or AD [see Figs. 5(a) and 5(b)] which would be expected to occur at $\hbar\omega\geq0.38$ MeV [see the above discussion of band 4]. The experimental Routhians [Fig. 5(c)] show that this band has a high excitation energy. Although all these observations argue in favor of a four-quasineutron band ($EFAB$), the suggested tentative signature of band 6 cannot be reconciled with this assignment. Similarly, the observed proton crossing at $\hbar\omega=0.54$ MeV would argue against a simple two-quasiproton configuration for this band.

In the next subsection, we shall discuss possible configurations for the strongly coupled bands 7 to 10. A summary of the proposed configuration assignments for all the bands in ^{172}Hf is given in Table V.

TABLE V. Summary of the configuration assignments for the rotational bands observed in ^{172}Hf in this study.

Band	Label	Configuration	(π,α)
1	(0)	Vacuum	(+,0)
2	(AE)	[633]7/2⊗[521]1/2	(−,1)
3	(BE)	[633]7/2⊗[521]1/2	(−,0)
4	(AF)	[633]7/2⊗[521]1/2	(−,0)
7	K=(14)	Band 8 ⊗ Band 10	(+,0)
8	K=6	$\nu([633]7/2\otimes[512]5/2)_{6-}$	(−,0)
9	K=6	$\pi([404]7/2\otimes[402]5/2)_{6+}$	(+,0)
10	K=8	$\pi([514]9/2\otimes[404]7/2)_{8-}$	(−,0)

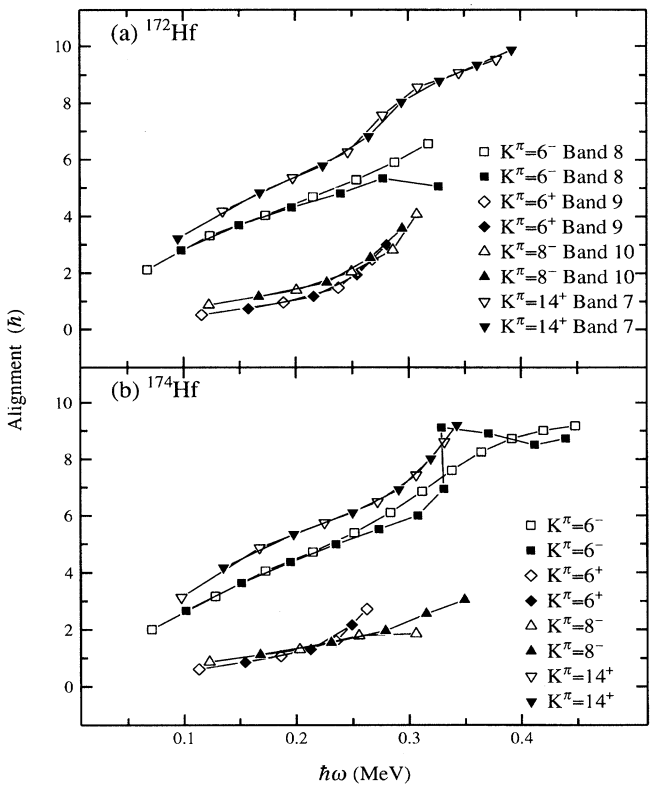

FIG. 7. Experimental alignments for the strongly coupled bands: (a) bands 7, 8, 9, and 10 in ^{172}Hf and (b) the $K^\pi=6^-$, $K^\pi=6^+$, $K^\pi=8^-$, and $K^\pi=14^+$ bands in ^{174}Hf. The Harris parameters $I_0=31.4\hbar^2$/MeV and $I_1=62.7\hbar^4$/MeV^3 were subtracted as a reference band. Open and closed symbols denote signature components $\alpha=1$ and 0, respectively.

Strongly coupled bands

Before discussing the configuration for the new high-K band 7, it is instructive to recall the configurations of the previously known high-K bands [1] in ^{172}Hf. Using systematics arguments, Walker *et al.* [1] have suggested the following configurations for bands 8, 9, and 10: (i) the two-quasineutron configuration $\nu\{[512]5/2\otimes[633]7/2\}_{6^-}$ for band 8; (ii) the two-quasiproton $\pi\{[404]7/2\otimes[402]5/2\}_{6^+}$ singlet state with possibly a very small admixture of the neutron $\nu\{[514]7/2\otimes[512]5/2\}_{6^+}$ configuration for band 9; and the $\pi\{[514]9/2\otimes[404]7/2\}_{8^-}$ two-quasiproton configuration for band 10. The structures of these three high-K bands are very similar to those built upon the corresponding isomeric states in ^{174}Hf [7,8], as seen from the plots of their experimental alignments in Fig. 7. Also shown in Fig. 7 are the alignment plots for band 7 in ^{172}Hf and the $K^\pi=14^+$ band in ^{174}Hf [7,8]. The similarity of these alignment curves suggests that the structure of band 7 may be understood by analogy with the $K^\pi=14^+$ band in ^{174}Hf which is described as a four-quasiparticle band formed by coupling of the $K^\pi=6^-$ and $K^\pi=8^-$ two-quasiparticle bands in the same nucleus.

Candidates for low-lying, high-K four-quasiparticle states in ^{172}Hf are $K^\pi=12^-$, $K^\pi=12^+$, and $K^\pi=14^+$ which are formed by various couplings of the $K^\pi=4^-$ (band 3) and $K^\pi=6^-$ (band 8) two-quasineutron configurations to the $K^\pi=6^+$ (band 9), and the $K^\pi=8^-$ (band 10) two-quasiproton configurations. (The $K^\pi=14^-$ configuration obtained by coupling of the $K^\pi=6^+$ and $K^\pi=8^-$ two-quasiproton configurations, both of which involve the [404]7/2 orbital, is not allowed by the Pauli principle.) The experimental DCO ratio for the 1255.9-keV linking transition to the ground-state band is consistent with both a $\Delta I=0$ and $\Delta I=2$ character and, hence, cannot be used to distinguish between the above three candidates. Also, lack of parity information for band 7 prevents us from making a definitive configuration assignment for this band. Finally, since both the $K^\pi=6^+$ and $K^\pi=8^-$ bands have similar alignments [see Fig. 7 (a)], combining their alignments with that of band 8 ($K^\pi=6^-$) would result in total alignment values that are nearly indistinguishable and are, both, in good agreement with the alignment of band 7. Likewise, the sum of alignments of bands 3 and 10 are quite close to that of band 7. The excitation energy of band 7, however, is more discriminating.

Walker *et al.* [5] have shown that the excitation energies of the four-quasiparticle states in the Hf nuclei are generally lower than the sum of the bandhead energies of their constituent two-quasiparticle states, presumably due to the proton-neutron interaction. Utilizing the bandhead energies of bands 3 and 7 through 10, and assuming a K value equal to the bandhead spin, we deduce a residual proton-neutron interaction of -104 keV (=3319–1417–2006), -224 keV (=3319–1685–1858), and -545 keV (=3319–2006–1858) for the $K^\pi=12^+$, 12^-, and 14^+ configurations for the bandhead state at 3319 keV, respectively. These values may be compared with the residual interactions of -199 and -172 keV for the $K^\pi=14^+$ and $K^\pi=12^-$ high-K bands in ^{174}Hf [7,8]. Therefore, a bandhead assignment of $K=12$ for the state from which the 1255.9-keV transition originates is in better agreement with the proton-neutron residual interactions observed in ^{174}Hf. This assignment, and the likely dipole characters of the 201.1 ($M1$) and 142.3 ($E1$) keV transitions result in an assignment of $K^\pi=(14^+)$ for band 7. (As mentioned before, the low-lying four-quasiproton $K^\pi=14^-$ configuration formed by coupling the $K=6^-$ and $K=8^-$ states violates the Pauli principle.) We can, therefore, assign $K^\pi=12^-$ to the bandhead state at 3319 keV which has the configuration of $\{\pi\{[402]5/2\otimes[404]7/2\}_{6^+}\otimes\nu\{[633]7/2\otimes[512]5/2\}_{6^-}\}_{12^-}$. The 201.1-keV transition is the first member of this high-K band.

The resulting residual interaction of the bandhead state of the strongly coupled high-K band 7 may be calculated in a similar manner. Assuming that this $K^\pi=14^+$ four-quasiparticle band is built upon the combination of the $K^\pi=8^-$ and $K^\pi=6^-$ two-quasiparticle states (bands 10 and 8) then the residual interaction is -201 keV (=3663–2006–1858). This is in excellent agreement with the residual interaction of -199 keV for the $K^\pi=14^+$ state in ^{174}Hf [7,8]. Figure 8(a) shows the experimental Routhian for band 7 (open squares) versus the sums of Routhians of bands 3 and 10 ($K^\pi=12^+$, dot-dashed line), bands 8 and 9 ($K^\pi=12^-$, dashed line), and bands 8 and 10 ($K^\pi=14^+$, solid line). This figure reveals that the best agreement with the experimental Routhian of band 7 is obtained with the $K^\pi=14^+$ assignment (solid line) from the sums of the experimental Routhians of

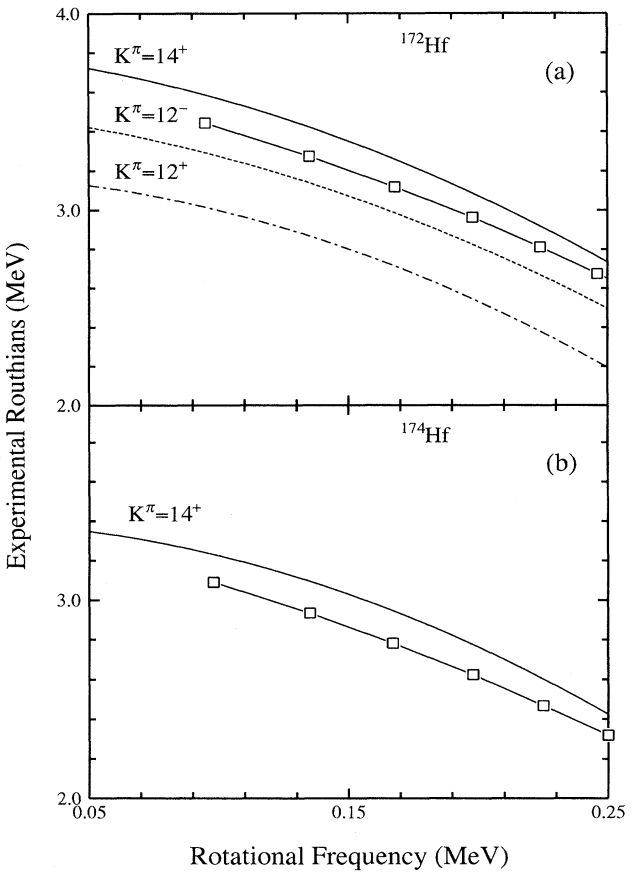

FIG. 8. (a) Comparison of the experimental Routhian for band 7 (open squares) versus the sums of Routhians for bands 3 and 10 (dot-dashed line), bands 8 and 9 (dashed line), and bands 8 and 10 (solid line) which correspond to a configuration assignment of $K^\pi=12^+$, 12^-, and 14^+, respectively. (b) shows the corresponding $K^\pi=14^+$ band (open squares) in ^{174}Hf with the sum of the $K^\pi=8^-$ and $K^\pi=6^-$ experimental Routhians (solid lines). These data are only shown up to a rotational frequency of 0.25 MeV because the lower-K bands are only observed below these frequencies.

the $K^\pi=8^-$ and $K^\pi=6^-$ states. Figure 8(b) shows the corresponding experimental Routhian plot for ^{174}Hf.

A very noteworthy feature of the $K^\pi=(12^-)$ bandhead state is that $24\pm9\%$ of the band intensity decays directly to the $I^\pi=12^+$ member of the ground state band via a single 1255.9-keV γ ray. The direct decay to the yrast state implies a $\Delta=K(12)$ transition which should be greatly hindered due to the K-selection rule for electromagnetic transitions. To some extent, the decay of this band resembles the decay of the $K^\pi=14^+$ isomeric state in ^{176}W which has two strong $M1$ branches with 6% and 33% to the yrast and yrare $I^\pi=14^+$ states ($K^\pi=0^+$), respectively [14]. In sharp contrast, the decay of the $K^\pi=14^+$, 4-μs isomeric state in ^{174}Hf has only a 1.1% direct $M1$ branch to the $I^\pi=14^+$ member of the yrast band via a 1291-keV transition [15]. The strong decay branches of this band are all to other high-K bands.

The decay of high-K isomeric states in this mass region is an unsettled issue which has been the subject of extensive discussion (see, e.g., [3,8,13–15]). These nuclei appear to dramatically change their structure from a deformation-aligned configuration to a rotationally-aligned configuration in a single γ-ray transition with a large change in K. Two mechanisms have been proposed to explain the apparent breakdown in the K-selection rule. The first mechanism involves the nuclear shape tunneling through the potential barrier in the γ degree of freedom and was proposed to explain the $\Delta K=25$ isomeric decay in ^{182}Os [13] and the decay of the $K=14$ isomer in ^{176}W [14]. In contrast, another mechanism was proposed [8,15] to explain the anomalous $\Delta K=14$ decay of the $K^\pi=14^+$ isomeric state in ^{174}Hf which decays directly to the yrast states ($K\approx0$). This decay was understood to be caused by the yrast band not having a pure $K=0$ structure at spin 12 because the Coriolis force can mix high-K components into its wave function. (Similar mixing arguments have also been employed [1,3] to explain the short lifetime of the isomeric $K^\pi=6^+$ state in ^{172}Hf.)

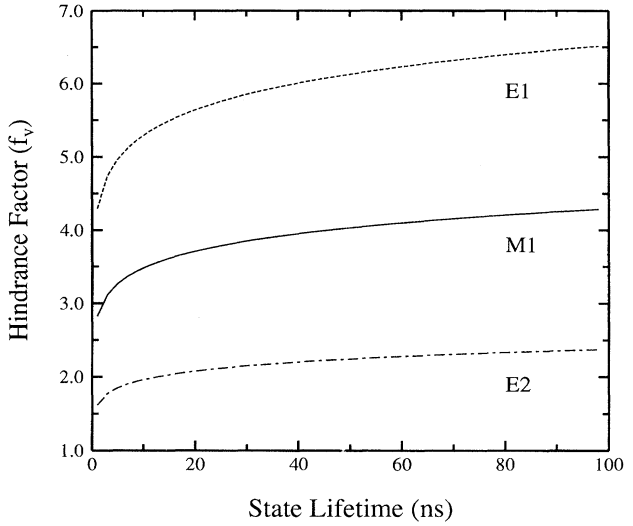

FIG. 9. Calculated reduced hindrance factors as a function of the lifetime of the $K^\pi=(12^-)$ bandhead state. The three curves from top to bottom correspond to the 1255.9 keV γ ray which links this band to the $I=12$ state in the ground state band being a [$\Delta I=0$, $E1$ (dashed line)], [$\Delta I=0$, $M1$ (solid line)], and a [$\Delta I=2$, $E2$ (dot-dashed line)] transition, respectively.

In order to compare the $\Delta K=(12)$ decay in ^{172}Hf with the $\Delta K=14$ decays in ^{174}Hf [8,15] and ^{176}W [14], it is instructive to consider the reduced hindrance factor defined as $f_\nu=\{T^\gamma_{1/2}/T^W_{1/2}\}^{1/\nu}$. ($T^\gamma_{1/2}$ is the partial γ-ray half-life and $T^W_{1/2}$ is the Weisskopf single-particle estimate.) Because of the unknown lifetime and the uncertainties in the spin and parity assignment of the $K^\pi=(12^-)$ bandhead state, we have calculated the reduced hindrance factors as a function of the state lifetime for three plausible spin-parity assignments. Figure 9 shows three curves which correspond to $E1$ (top, dashed line), $M1$ (middle, solid line), and $E2$ (bottom, dot-dashed line) character for the 1255.9-keV linking transition. (They correspond to the assumption of $K^\pi=12^-$, 12^+, and 14^+ for the bandhead state, respectively.) Assuming an upper limit estimate of 20 ns for the lifetime of the bandhead state, we obtain 6.1 ($E1$), 4.0 ($M1$), and 2.2 ($E2$) as the approximate upper limits on the hindrance factors for the 1255.9-keV transition. As seen in Fig. 9, the above estimates will change only slightly if the lifetime of the bandhead state

TABLE VI. Comparison of the reduced hindrance factors for the K-forbidden $M1$ and $E2$ decays from the high-K bands to the ground-state (G), aligned superband (S), and 0_2^+ (β) bands in ^{172}Hf , ^{174}Hf [15], and ^{176}W [16]. The character and multipolarity of each transition is also indicated.

	Initial	f_ν for decay to final state				
(A,Z)	K^π	$(14^+)_G$	$(12^+)_G$	$(14^+)_S$	$(12^+)_S$	$(12^+)_\beta$
^{172}Hf	(12^-)		≤ 6.1 ($E1$)			
^{174}Hf	14^+	5.7 $M1$	5.5 $E2$		>3.7 $E2$	4.5 $E2$
^{176}W	14^+	3.6 $M1$	>3.2 $E2$	3.0 $M1$	>2.9 $E2$	2.3 $E2$

were to change by a factor of 2. (The recoils possess a velocity of $v/c \approx 2\%$ and rapidly move out of the focus of all but the backward-angle Ge detectors in the array. Therefore, γ rays emitted from a much longer-lived state would have been seriously attenuated or become undetectable.) Thus, for the most likely assignment of $K^\pi=(12^-)$, we deduce a reduced hindrance factor of ≈ 6.1 for the 1255.9-keV ($E1$) transition to the yrast band. In Table VI, this estimate is compared with the reduced hindrance factors for the $M1$ and $E2$ decay transitions from the $K^\pi=14^+$ isomeric states to the ground state, S and "β" (0_2^+) bands in ^{174}Hf [15] and ^{176}W [16]. The estimated $f_\nu \approx 6.1$ for the 1255.9-keV transition in ^{172}Hf is somewhat larger than the values of $f_\nu=5.7$ and 3.6 for the corresponding $M1$ transitions to the yrast bands in ^{174}Hf and ^{176}W, respectively. It is interesting to note that the f_ν values shown in Table VI are larger for the $E2$ transitions to the ground state bands than those to either the S or "β" bands. While the smaller hindrance factors for transitions to the aligned S band may be explained in terms of the K-mixing mechanism, those to the "β" bands are not easily explainable. Recently, evidence has been presented for a new interpretation of the β-vibrational bands as two-phonon γ-vibrational bands [17]. This interpretation provides an appealing explanation for the small hindrance factors observed for transitions from the high-K bands to the 0_2^+ states as due to the γ-tunneling effect. The observed f_ν values, therefore, may provide evidence that both K-mixing and γ-tunneling mechanisms are present and play an important role in circumventing the K-selection rule. The K-mixing is important for the decay to the aligned S band, while the γ-tunneling mechanism is needed for the decay to the 0_2^+ band. Interestingly, the f_ν for the $E2$ transition to the S band is smaller (larger) than the one for the 0_2^+ band in ^{174}Hf (^{176}W). This would be expected since the potential energy surfaces in ^{176}W are softer with respect to γ vibrations than those in ^{174}Hf.

In ^{172}Hf, only the decay of the $K^\pi=(12^-)$ state to the yrast band in the region of the first band crossing is observed. Since the TRS calculations (Fig. 3) do not provide any evidence for γ softness in ^{172}Hf, it is likely that the apparent breakdown of the K-selection rule is caused more by the K-mixing mechanism, similar to the decay of the $K^\pi=14^+$ state to the S band in ^{174}Hf.

It should be noted that this interpretation in terms of the Coriolis force and band mixing may not be the sole explanation for the apparent breakdown of the K selection rule. To fully understand the decay of the $K^\pi=(12^-)$ bandhead, more theoretical calculations are required (for example, tilted axis cranking calculations [18] which were employed in the explanation of the $K^\pi=14^+$ isomer decay in ^{174}Hf [15]).

V. CONCLUSIONS

We have extended the known level scheme of ^{172}Hf from spin 34 to spin 44$\hbar$ and five new rotational bands have been established. A new band was observed to cross the lowest negative-parity band. These bands interact weakly and the negative-parity band was extended above the crossing region. One of the other newly established bands is a high-K strongly coupled rotational band. This band is likely to be built upon a $K^\pi=(14^+)$ bandhead state. Another newly established bandhead state from a $K^\pi=(12^-)$ strongly coupled band decays predominantly to the yrast 12^+ state with a single, $\Delta K=(12)$, 1255.9-keV γ ray. The apparent breakdown of the K-selection rule for this bandhead state is likely caused by the mixing of high-K components into the yrast band in the region of the first band crossing where the feeding takes place.

ACKNOWLEDGMENTS

The authors would like to thank P.M. Walker for many helpful discussions and also D.C. Radford for the use of the "Radware" software [6]. The Nuclear Structure Research Laboratory at Rochester is supported by the NSF under Contract No. PHY-9220318. Oak Ridge National Laboratory is managed for the U.S. Department of Energy by Martin Marietta Energy Systems, Inc. under Contract No. DE-AC05-84OR21400. The University of Tennessee is sponsored by the Department of Energy, Nuclear Physics Division under Contract No. DE-FG05-87ER40361.

[1] P.M. Walker, G.D. Dracoulis, A. Johnson, and J.R. Leigh, Nucl. Phys. **A293**, 481 (1977).

[2] E.S. Paul, R. Chapman, J.C. Lisle, J.N. Mo, S. Sergiwa, J.C. Willmott, and A. Holm, J. Phys. G **11**, L53 (1985).

[3] P.M. Walker, G.D Dracoulis, A.P. Byrne, T. Kibédi, and A.E. Stuchbery, Phys. Rev. C **49**, 1718 (1994).

[4] R. Chapman, J. Irwin, J.C. Lisle, J.N. Mo, J. Copnell, C. Tenreiro, G.S. Li, G.J. Yuan, and P.M. Walker, Daresbury Lab., 1990-1991 Annual Report, Appendix, p. 33 (1991).

[5] P.M. Walker, Phys. Scr. **T5**, 29 (1983), and references therein.

[6] D.C. Radford, in Proceedings of the 1989 International Nuclear Physics Conference, Sao Paulo, Brazil, 1989.

[7] N.L. Gjørup, G. Sletten, P.M. Walker, M.A. Bentley, D.M. Cullen, J.F. Sharpey-Schafer, P. Fallon, and G. Smith, in Proceedings of International Conference on Nuclear Structure at High Angular Momentum, Ottawa, 1992, AECL-10613, p. 160.

[8] N.L. Gjørup, Ph.D. thesis, University of Copenhagen, Den-

mark, 1994; N.L. Gjørup, P.M. Walker, G. Sletten, M.A. Bentley, B. Fabricius, and J.F. Sharpey-Schafer, Nucl. Phys. **A582**, 369 (1995).

[9] T.L. Khoo, F.M. Bernthal, R.G.H. Robertson, and R.A. Warner, Phys. Rev. Lett. **37**, 823 (1976); T.L. Khoo, F.M. Bernthal, R.A. Warner, G.F. Bertsch, and G. Hamilton, *ibid.* **35**, 1256 (1975); T.L. Khoo, J.C. Waddington, R.A. O'Neil, Z. Preibisz, D.G. Burke, and M.W. Johns, *ibid.* **28**, 1717 (1972).

[10] W. Nazarewicz, R. Wyss, and A. Johnson, Nucl. Phys. **A503**, 285 (1989).

[11] C. Baktash *et al.* (unpublished).

[12] C. Baktash, M.L. Halbert, D.C. Hensley, N.R. Johnson, I.Y. Lee, J.M. McConnell, F.K. McGowan, C.M. Steele, M.P. Carpenter, V.P. Janzen, and L.L. Reidinger, 1988 Oak Ridge National Lab., Annual Report, p. 72.

[13] P. Chowdhury *et al.*, Nucl. Phys. **A485**, 136 (1988).

[14] B. Crowell *et al.*, Phys. Rev. Lett. **72**, 1164 (1994).

[15] P.M. Walker *et al.*, Phys. Rev. Lett. **65**, 416 (1990).

[16] B. Crowell *et al.*, Phys. Rev. C (submitted).

[17] R.F. Casten and P. von Brentano, Phys. Rev. C **50**, R1280 (1994).

[18] S. Frauendorf, Phys. Scr. **24**, 349 (1981); Nucl. Phys. **A557**, 259c (1983).